REVIEW ARTICLE

The Current State of Research on Deformation, Strain, and Velocity across the Alpine-Himalayan Belt Using Transcontinental Sentinel-1 InSAR and GNSS

Mohit Sheode*

Department of Civil Engineering, Maulana Azad National Institute of Technology Bhopal, India

*Corresponding author: mhtsht@gmail.com

ORCID: https://orcid.org/0009-0009-5719-5084

Abstract

Research on present-day deformation across the Alpine-Himalayan belt has crossed a methodological threshold. Regional Sentinel-1 studies in Anatolia, Iran, and Tibet have now been joined by the first transcontinental three-dimensional velocity and horizontal strain-rate field, derived from more than 222,000 radar images acquired during 2016-2024 and a belt-wide GNSS compilation. The result provides approximately 1 km sampling over more than 20 million km² and 11,000 km of active continental deformation. This review assesses what those advance changes scientifically, and what it does not. The emerging belt-wide picture is neither a rigid-block system nor a uniformly deforming continuum. Strain is sharply localized on the North Anatolian, Haiyuan, Kunlun, and related faults, along the Himalayan and Pamir convergence fronts, and within Tibetan rifts; elsewhere, shortening, shear, and extension are distributed across broad interiors. Horizontal velocities are mainly tectonic, whereas much of the short-wavelength vertical field records aquifer depletion, sediment compaction, permafrost change, landsliding, or other shallow processes. The main limitations now arise from how observations are combined: line-of-sight geometry, uneven GNSS density, reference-frame and epoch differences, correlated atmospheric errors, phase unwrapping, regularization, and the treatment of fault creep and post seismic motion. Consequently, kilometer-scale pixels do not imply kilometer-scale independent resolution, and a strain anomaly cannot be equated directly with locked-fault hazard. The next phase should move from static average velocities toward uncertainty-aware four-dimensional models that combine C- and L-band radar, denser GNSS, explicit fault discontinuities, and process-based separation of tectonic and non-tectonic deformation.

Keywords: Alpine-Himalayan belt; Sentinel-1; InSAR; GNSS; crustal deformation; strain rate; velocity field; tectonic geodesy

Journal-status statement: It is not under-review at any journal. Subsequent versions may contain substantial revisions arising from community feedback / submission to journal(s). Co-author(s) may be included in future versions. Feedback is welcome & please feel free to contact the author for the same (via email only). PRE-PRINT VERSION (I): 31.08.2026

THIS MANUSCRIPT IS A NON-PEER-REVIEWED PREPRINT SUBMITTED TO EARTHARXIV.

1. Introduction

The Alpine-Himalayan belt is not one plate boundary in the usual sense. It is an 11,000 km-wide chain of collisions, subduction zones, strike-slip systems, extensional provinces, and deforming plate interiors extending from southwestern Europe to eastern China. Across it, Nubia, Arabia, and India converge with Eurasia, but the surface response changes from Alpine uplift and Apennine extension to Anatolian escape, Caucasian and Zagros shortening, Pamir indentation, Tibetan extension, and Himalayan under thrusting [1-5]. A single tectonic label therefore hides the question that geodesy must answer: where is motion accommodated, over what width, and by which mixture of elastic loading, aseismic slip, distributed deformation, and non-tectonic ground motion?

Until recently, this question could be addressed at continental scale only with Global Navigation Satellite System (GNSS) velocities. GNSS provides stable three-component motion in a defined terrestrial reference frame, but station spacing varies from a few kilometers in parts of Europe and Turkey to tens or hundreds of kilometers across Iran, Afghanistan, the Pamir, Tibet, and much of the Himalaya. Such spacing is adequate for plate-scale kinematics but can miss velocity gradients across individual faults or falsely concentrate strain around clusters of stations [2-4]. Sentinel-1 changed the sampling problem. Its repeated C-band radar observations can recover line-of-sight (LOS) motion across large areas at dense spatial intervals, and automated systems now process the volume of imagery needed for continental time-series analysis [6,7].

The decisive development is the 2026 transcontinental synthesis by Elliott et al. [1]. More than 222,000 Sentinel-1 images acquired between 2016 and 2024 were combined with a new GNSS compilation in a Eurasia-fixed frame to produce average east, north, and vertical velocities and horizontal strain rates at approximately 1 km sampling across more than 20 million km². In parallel, Castro-Perdomo et al. [2] combined 42 published GNSS velocity fields into 11,177 horizontal and 3,940 vertical station velocities and estimated strain and its posterior uncertainty across the belt. These products mark the transition from a mosaic of regional experiments to a common transcontinental measurement framework.

Three quantities require separation at the outset. Deformation is the observed change in position or shape; velocity is the rate fitted to a displacement time series; and strain rate is a spatial derivative of a velocity field. A radar pixel measures none of these in full three dimensions. It measures phase change projected onto the satellite LOS, after corrections and referencing. Three-dimensional velocity is

Journal-status statement: It is not under-review at any journal. Subsequent versions may contain substantial revisions arising from community feedback / submission to journal(s). Co-author(s) may be included in future versions. Feedback is welcome & please feel free to contact the author for the same (via email only). PRE-PRINT VERSION (I): 31.08.2026

THIS MANUSCRIPT IS A NON-PEER-REVIEWED PREPRINT SUBMITTED TO EARTHARXIV.

reconstructed from multiple LOS geometries and GNSS constraints, while strain is inferred after interpolation, differentiation, and regularization. Each step changes the effective resolution and the uncertainty. The current literature is strongest when it states these dependencies explicitly and weakest when a dense-looking map is treated as a direct observation of fault locking or seismic hazard.

1.1 Review approach and scope

This is a critical narrative review rather than a systematic review or meta-analysis. The evidence base is anchored by the 2026 transcontinental Sentinel-1-GNSS synthesis [1] and the 2025 belt-wide GNSS strain compilation [2], and is evaluated against the regional InSAR-GNSS and methodological studies cited throughout the article. Studies were retained when they (i) report present-day velocity or horizontal strain within the Alpine-Himalayan belt, (ii) describe InSAR-GNSS fusion, referencing, uncertainty, or strain estimation, or (iii) document transient or non-tectonic signals that can bias interseismic interpretation. The cited corpus spans 2000-2026, with emphasis on the Sentinel-1 era (2015-2026); earlier GNSS and methodological studies are included where they provide long-term kinematic or inversion context. Because the corpus was assembled for critical synthesis rather than through a preregistered exhaustive search, no PRISMA-style study counts or claim of meta-analytic completeness is made.

The review focuses on present-day interseismic velocity and strain. Co-seismic and post seismic deformation enter only where they can contaminate an average velocity or clarify the origin of a mapped gradient. The central assessment is that observational coverage has become transcontinental, but interpretation remains scale-dependent and regionally uneven.

2. From regional demonstrations to a belt-wide field

The transcontinental product rests on a decade of regional demonstrations. In Anatolia, Weiss et al. [8] showed that five years of Sentinel-1 observations, processed across 40 overlapping frames and tied to GNSS, could recover the westward motion of Anatolia, the narrow gradient across the North Anatolian Fault (NAF), and non-tectonic subsidence in the Konya Basin. In northeast Tibet, Ou et al. [9] derived east and vertical velocities at about 100 m spacing and approximately 1 mm/yr accuracy over 440,000 km², then formed a roughly 1 km strain-rate field. In Iran, Watson et al. [10] processed seven years of data to construct a 500 m country-scale east-vertical field over 1.7 million km². Plateau-wide and subregional work subsequently extended three-dimensional reconstruction across Tibet [11], the southern Tibetan rifts [12], and the southeastern plateau [13].

These studies solved different parts of the same problem. Anatolia demonstrated that dense radar observations could transform a patchy GNSS strain map into a spatially coherent fault-parallel belt. Iran showed that the method also works where tectonic gradients are broad and groundwater signals are abundant. Tibetan studies confronted the additional effects of elevation-dependent atmosphere, snow, permafrost, sparse GNSS, and strong topography. Their methods were then portable enough to be applied across the entire Alpine-Himalayan belt.

The present state should therefore be described carefully. A belt-wide data product exists, but a uniformly resolved belt-wide tectonic model does not. The 1 km grid gives a common sampling framework. Independent resolving power still varies with radar coherence, track geometry, GNSS density, time-series length, fault orientation, and the scale of smoothing. Regional models remain indispensable for testing whether a transcontinental anomaly is a fault, a broad strain zone, a transient, or a shallow surface process. Figure 1 locates the regional domains used in this synthesis and distinguishes reported strain-rate ranges from areas for which no single comparable value is available.

Journal-status statement: It is not under-review at any journal. Subsequent versions may contain substantial revisions arising from community feedback / submission to journal(s). Co-author(s) may be included in future versions. Feedback is welcome & please feel free to contact the author for the same (via email only). PRE-PRINT VERSION (I): 31.08.2026

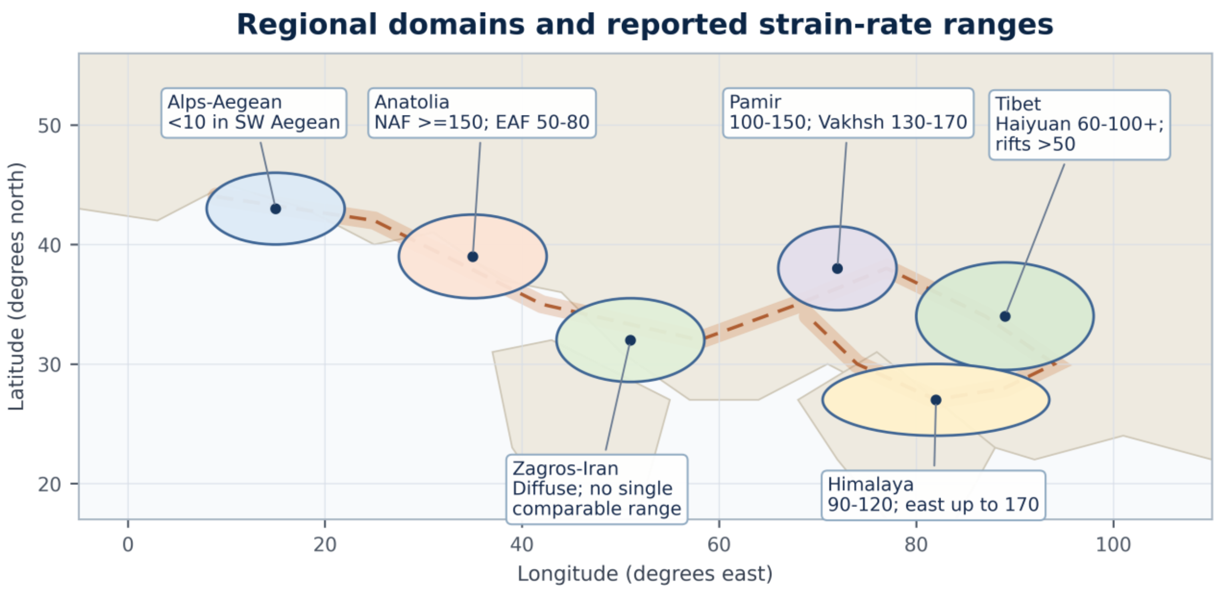

Figure 1. Schematic index map of the regional domains discussed across the Alpine-Himalayan belt. Geographic positions and the belt corridor are schematic; the labels summarize values compiled from the cited studies rather than a reprocessed geodetic surface. Unit: nano strain per year.

Source: synthesis from [2,8,9,12].

3. Observational and analytical architecture

3.1 Sentinel-1 time-series construction

Continental InSAR begins with repeated Sentinel-1 acquisitions grouped into overlapping ascending and descending frames. LiCSAR automates orbit application, co-registration, interferogram formation, topographic-phase removal, geocoding, and unwrapping; LiCSBAS forms small-baseline networks, screens unreliable interferograms and pixels, inverts displacement histories, and estimates average LOS velocities [6,7]. The transcontinental study used 2016-2024 imagery at approximately 1 km output spacing [1]. Regional projects often retain finer grids. The Iran study, for example, formed about 85,000 interferograms from about 18,500 acquisitions on 19 tracks, applied GACOS tropospheric corrections, rejected interferograms using loop closure, and estimated velocities at 0.005 degrees (approximately 500 m) [10].

Dense sampling is obtained only after aggressive quality control. Interferometric networks must bridge acquisition gaps without allowing temporal baselines to destroy coherence. Pixels affected by low coherence, unwrapping failure, radar shadow, or layover are masked. Residual topography-correlated phase is removed or down weighted, and long-wave ramps are estimated during frame mosaicking. Atmospheric corrections reduce stratified delays but do not remove all turbulent structure. Averaging many interferograms suppresses random atmospheric noise; it cannot guarantee removal of a seasonal signal that is correlated with topography or sampling.

C-band coherence remains geographically selective. Bare, arid surfaces across Anatolia, Iran, and much of Tibet are favorable, while forests, irrigated plains, snow, glaciers, monsoon vegetation, and unstable slopes create gaps. High relief adds geometric distortion exactly where many active Himalayan faults and landslides occur. Thus, the absence of a velocity gradient can mean low deformation, insufficient sensitivity, or a mask. A defensible map must carry the valid-observation density and uncertainty alongside the velocity.

3.2 GNSS compilation, epochs, and reference frames

GNSS supplies what InSAR lacks: absolute three-component motion in a terrestrial frame and strong sensitivity to north-south displacement. Combining published GNSS fields is nevertheless a geodetic analysis in its own right. Castro-Perdomo et al. [2] filtered post seismic stations and statistical outliers, transformed input solutions to ITRF2014 with six-parameter Helmert transformations, combined collocated solutions using robust statistics, and then rotated the field into Eurasian and other tectonic frames. The mean alignment residual across input fields was 0.5 ± 0.3 mm/yr. Vertical velocities were handled separately and were not used in their two-dimensional strain inversion because vertical records were less complete and not transformed in the same way.

Reference-frame choice is not bookkeeping. A Eurasia-fixed frame makes the broad collision visible, but a central Tibet-fixed frame exposes east-west extension and internal motion around the eastern Himalayan syntaxis more clearly [2]. An offset or ramp of only a few millimeters per year can create a continent-scale strain artefact when differentiated. Continental mosaics therefore require overlapping GNSS ties, explicit frame uncertainty, and checks for residual spatial patterns rather than a single network-wide root-mean-square statistic [17].

Journal-status statement: It is not under-review at any journal. Subsequent versions may contain substantial revisions arising from community feedback / submission to journal(s). Co-author(s) may be included in future versions. Feedback is welcome & please feel free to contact the author for the same (via email only). PRE-PRINT VERSION (I): 31.08.2026

THIS MANUSCRIPT IS A NON-PEER-REVIEWED PREPRINT SUBMITTED TO EARTHARXIV.

Epoch consistency is equally important. Published GNSS velocities may span different years, while the Sentinel-1 average spans 2016-2024. Large earthquakes inside or near that window include the 2023 Türkiye-Syria sequence and several Tibetan and Himalayan events. A nominally interseismic field can retain after slip or viscoelastic relaxation for years to decades. Removing stations within a fixed epicentral radius is a useful first pass, but it does not remove long-wavelength, long-lived transients.

3.3 Three-dimensional fusion and strain estimation

An LOS velocity is the projection of east, north, and vertical motion onto the radar look vector. Ascending and descending observations provide two equations, but their near-polar orbits leave the north component weakly observed. A common solution interpolates GNSS north velocities, then decomposes the two LOS fields into east and vertical components. More general joint inversions solve simultaneously for a spatial velocity model using the LOS and GNSS observations with uncertainty-based weights [14-16]. These approaches preserve short-wavelength InSAR detail while allowing GNSS to anchor the long wavelengths and reference frame.

VELMAP-style inversions divide the surface into spherical triangles, assume that velocity varies linearly within each triangle, and derive velocity, rotation, and strain at the mesh nodes [8,38]. Body-force approaches instead represent a smoothly deforming elastic sheet and can include velocity discontinuities associated with surface creep [2]. Both require regularization. Strong smoothing suppresses noise but broadens fault zones and lowers peak strain; weak smoothing sharpens gradients but may turn atmospheric or hydrologic residuals into apparent tectonic structure. The GNSS synthesis used nominal node spacing near 100 km in poorly instrumented regions and refined it to 15 km, or about 5 km in focused inversions, where station density allowed [2].

Horizontal strain rate is the symmetric spatial gradient of horizontal velocity. It can be expressed through principal shortening and extension, dilatation, maximum shear, or a tensor norm. These quantities are related but not interchangeable. Even a factor-of-two difference can arise when a study compares engineering shear with a fault-parallel velocity gradient [8]. More fundamentally, differentiation amplifies short-wavelength noise. The effective resolution of a strain map is controlled by the inversion mesh, covariance model, filter, and station geometry, not by the displayed radar pixel size.

Journal-status statement: It is not under-review at any journal. Subsequent versions may contain substantial revisions arising from community feedback / submission to journal(s). Co-author(s) may be included in future versions. Feedback is welcome & please feel free to contact the author for the same (via email only). PRE-PRINT VERSION (I): 31.08.2026

THIS MANUSCRIPT IS A NON-PEER-REVIEWED PREPRINT SUBMITTED TO EARTHARXIV.

3.4 Uncertainty is part of the field, not an appendix

Current best practice estimates uncertainty at each stage: time-series velocity error, frame-tie residuals, GNSS covariance, decomposition uncertainty, and the posterior spread of the strain inversion. Bootstrap estimates are useful for LOS velocity, while Bayesian or ensemble inversions can sample alternative smoothing strengths [2,10,32]. Coordinate distortion must also be tested over a domain this large. A synthetic rigid-plate experiment in the 2025 GNSS study produced spurious strain below 5 nano strain/yr, small compared with the main belts but not negligible in stable interiors [2].

Formal uncertainty alone is insufficient when the model is wrong. Correlated atmospheric errors, an unmodelled velocity step across a creeping fault, or post seismic motion shared by neighboring stations can leave low formal errors and a biased strain field. Residual-vector maps, cross-validation by withholding stations or tracks, and comparison across model classes are more informative than one preferred solution.

4. The belt-wide kinematic picture

The clearest result of transcontinental mapping is a mixed mode of deformation. Major faults and collision fronts produce narrow, high-gradient belts, yet broad regions between them also deform. The same data therefore reject two over-simple descriptions: the belt is neither a set of perfectly rigid blocks nor a smooth continuum. Localization and distributed strain coexist, and their apparent proportion changes with spatial scale [1,2,11,13].

4.1 Alps, Apennines, Aegean, and western Anatolia

At the western end, horizontal rates are generally lower than along Anatolia or the India-Asia collision, while vertical motion is prominent. GNSS records approximately 1-2.5 mm/yr uplift along the Alps [2,20]. That signal is not a simple measure of active shortening: glacial isostatic adjustment, erosion, buoyancy, slab processes, and tectonics can all contribute. The Po Basin shows subsidence exceeding 5 mm/yr in places, produced by a mixture of compaction, groundwater use, and deeper geodynamics, whereas parts of the central Apennines combine uplift with positive dilatation [2]. The lesson resembles the transcontinental vertical field more broadly: vertical velocity is rich in process information but cannot be labelled tectonic without auxiliary evidence.

Journal-status statement: It is not under-review at any journal. Subsequent versions may contain substantial revisions arising from community feedback / submission to journal(s). Co-author(s) may be included in future versions. Feedback is welcome & please feel free to contact the author for the same (via email only). PRE-PRINT VERSION (I): 31.08.2026

THIS MANUSCRIPT IS A NON-PEER-REVIEWED PREPRINT SUBMITTED TO EARTHARXIV.

Toward the Aegean and western Anatolia, extension becomes the dominant horizontal signal. The refined GNSS field shows a transition from east-west extension in central Anatolia to north-south extension in the Western Anatolian Extensional Province, while the North Aegean shear belt widens westward [2,21]. Parts of the southwestern Aegean remain below 10 nano strain/yr and behave comparatively rigidly. Offshore geometry limits InSAR coverage, so GNSS, seafloor geodesy, and earthquake mechanisms remain necessary for the Hellenic and Cyprus subduction systems.

4.2 Anatolia and the Caucasus

Anatolia remains the clearest demonstration of what InSAR adds to GNSS. Relative to Eurasia, the region moves westward at roughly 20-25 mm/yr, while the NAF accommodates right-lateral motion of about 20-30 mm/yr and the East Anatolian Fault (EAF) carries a smaller left-lateral component [2,8]. The InSAR-GNSS model maps strain rates of at least 150 nano strain/yr along nearly the full NAF, rather than the discontinuous high-strain patches obtained from GNSS alone [8]. The EAF is a weaker but distinct shear belt, commonly 50-80 nano strain/yr in the newer GNSS synthesis, with values above 100 nano strain/yr near the Karliova triple junction [2].

High strain on a fault is not automatically stored elastic strain. At the Ismetpasa segment, failing to represent surface creep can generate apparent strain above 300 nano strain/yr [2]. Post seismic motion after the 1999 Izmit and 2023 Kahramanmaras earthquakes may persist within velocities classified as interseismic. Hazard interpretation therefore requires a model that distinguishes locked-fault loading, surface creep, after slip, and viscoelastic relaxation rather than assigning all observed velocity gradient to one mechanism.

The Greater Caucasus shows north-south to NNE-SSW shortening that increases eastward toward the Caspian Sea and exceeds 60 nano strain/yr in the GNSS synthesis [2]. The Lesser Caucasus contains discontinuous zones of shortening, extension, and strike-slip motion. These patterns agree with regional geology, but station coverage north of the Greater Caucasus and around the Caspian remains too sparse for fault-scale conclusions.

4.3 Iran, the Zagros, and the Makran transition

Arabia-Eurasia convergence is distributed across the Zagros, central Iran, the Alborz, Kopet Dagh, and eastern Iran before reaching the Makran subduction zone. The first country-scale InSAR-GNSS field shows predominantly diffuse deformation, punctuated by localized gradients on the North Tabriz, Main Kopet Dagh, Main Recent, Sharoud, and Doruneh faults [10]. The central Iranian Plateau has low internal deformation in the preferred model, although parts of the Dasht-e Kavir must be masked because sediment motion and phase bias can imitate crustal velocity. This is a useful counterexample to the assumption that aridity guarantees an uncomplicated radar surface.

Vertical rates across Iran are dominated locally by aquifer depletion, sometimes accompanied by horizontal motion and flexural uplift around subsidence bowls [10]. These signals are scientifically valuable but dangerous in a strain calculation because horizontal gradients around a groundwater basin can overlap active faults. Along the Makran coast, incomplete offshore sampling further separates the observed land field from the plate-boundary process that drives it. The priority here is not merely denser mapping but joint hydrologic, tectonic, and offshore constraint.

4.4 Pamir, Tian Shan, and Tibet

The India-Asia collision zone contains the belt's strongest combination of shortening, strike-slip shear, and internal extension. GNSS-derived dilatation reaches approximately -60 to -100 nano strain/yr across the Pamir thrust system, while refined strain norms reach 100-150 nano strain/yr and rise to 130-170 nanostrain/yr on the Vakhsh Fault. The central Tian Shan commonly records 50-60 nano strain/yr, with local peaks near 100 nanostrain/yr [2]. Sparse stations and steep terrain make these values more scale-dependent than equally large values in well-instrumented Anatolia.

Across Tibet, the block-versus-continuum debate has become a question of wavelength. Plateau-wide decomposition finds discontinuous short-wavelength motion associated with faults, post seismic deformation, and surface processes, but smoother long-wavelength uplift and subsidence [11,36]. High-resolution strain concentrates on the Altyn Tagh, Kunlun, Haiyuan, Xianshuihe-Xiaojiang, Jiali, and related systems [2,9,18,19,38]. Between these faults, measurable internal strain remains. In southeastern Tibet, models that allow deformable blocks fit substantial distributed strain better than a rigid-block end member [13]. The observations favour a hybrid crust in which faults organize motion without absorbing all of it.

Northeast Tibet provides the sharpest example of scale dependence. A GNSS-only synthesis places the Haiyuan Fault near 60 nano strain/yr, with local values around 80, while the approximately 1 km Sentinel-1 strain map exceeds 100 nano strain/yr and surpasses 400 nano strain/yr on a creeping section

[2,9]. The disagreement is not simply an error; the models are resolving different widths and treating creep differently. The InSAR field also images shear on the East Kunlun Fault, contraction at fault junctions and within the Qilian Shan, and previously unmapped deforming structures [9,19].

Southern Tibet is extensional despite the continental collision. Sentinel-1 observations from 2015-2022 combined with GNSS reveal dilatation focused along seven north-south rifts and a summed decadal extension of 18.4 ± 1.7 mm/yr [12]. Local dilatation above 50 nano strain/yr is higher than broad GNSS-only estimates, again showing what dense LOS data add. At the same time, permafrost thaw, seasonal freeze-thaw, hydrology, and unwrapping errors can produce larger vertical rates than the tectonic signal [33,34]. Multi-scale separation helps, but no wavelength threshold maps uniquely onto a physical process.

4.5 The Himalayan arc and eastern syntaxis

The Himalayan arc is dominated by arc-normal shortening above the Main Himalayan Thrust (MHT). In the belt-wide GNSS synthesis, strain rates commonly fall between 90 and 120 nano strain/yr and rise to about 140 nano strain/yr, with peaks near 170, in the eastern Himalayan syntaxis [2]. Longer GNSS records across Kashmir-Himachal, Garhwal, Kumaun, and Nepal show that convergence and locking vary along strike rather than following one uniform coupling profile [22,25-27]. High-resolution Nepal work is beginning to connect the velocity field to a geodetic moment budget [25].

Obliquity adds an arc-parallel component. GPS, structural observations, and regional kinematics show stronger partitioning in the northwest Himalaya and near the syntaxes, where strike-slip and transverse faults redirect part of the convergence while thrust systems absorb most arc-normal shortening [22,23,26]. The Karakoram Fault is important but not a uniformly narrow strain sink; current geodetic estimates support variable localization and substantial deformation elsewhere [26].

The Himalaya remains less uniformly resolved by Sentinel-1 than dry Tibet. Snow, vegetation, monsoon moisture, radar shadow, and rapid slope motion remove or contaminate C-band phase, while north-south convergence is the component to which near-polar radar is least sensitive. In addition, overriding-plate deformation can bias coupling estimates if all interseismic velocity is attributed to slip deficit on the MHT [24]. GNSS is therefore not merely a calibration layer here; it carries the component most needed to interpret the collision.

Journal-status statement: It is not under-review at any journal. Subsequent versions may contain substantial revisions arising from community feedback / submission to journal(s). Co-author(s) may be included in future versions. Feedback is welcome & please feel free to contact the author for the same (via email only). PRE-PRINT VERSION (I): 31.08.2026

THIS MANUSCRIPT IS A NON-PEER-REVIEWED PREPRINT SUBMITTED TO EARTHARXIV.

4.6 Regional synthesis

Table 1. Regional deformation patterns and the present observational bottleneck.

Domain	Dominant kinematics	What joint InSAR-GNSS resolves	Main unresolved issue
Alps-Apennines	Low-to-moderate horizontal deformation; uplift, extension, and basin subsidence	Separates broad horizontal strain from short-wavelength vertical motion	Tectonic uplift versus glacial, erosional, hydrologic, and compaction signals
Aegean-Anatolia	Western extension; NAF and EAF strike-slip shear	Continuous fault gradients, creeping segments, and anthropogenic subsidence	Creep, afterslip, and locked-fault strain must be separated
Caucasus-Iran	Collision-related shortening with strike-slip and broad distributed strain	Country-scale gradients across mapped and previously subtle fault zones	Sparse GNSS, Caspian/Makran offshore gaps, and groundwater contamination
Pamir-Tian Shan	Strong shortening and localized shear around indenter margins	Sharper strain belts than GNSS interpolation alone	Harsh terrain, uneven stations, and persistent earthquake transients
Tibetan Plateau	Localized strike-slip plus distributed internal strain and E-W extension	Fault-scale strain, rift extension, and multi-wavelength deformation	Atmosphere, permafrost, unwrapping, reference frame, and smoothing scale
Himalayan arc	Arc-normal shortening with segment-dependent arc-parallel partitioning	MHT loading context and regional velocity gradients where coherence permits	Weak N-S radar sensitivity, decorrelation, and overriding-plate deformation
Eastern syntaxis-SE Tibet	Clockwise rotation, lateral transport, strike-slip shear, and diffuse strain	Tests rigid-block, deformable-block, and continuum models at common scale	Fault completeness, transient signals, and model non-uniqueness

Sources synthesized from [1,2,8-13,20-27].

4.7 Quantitative comparison of reported strain rates

Table 2 and Figure 2 consolidate the numerical strain-rate statements reported in Sections 4.1-4.5. They are retrieval aids, not a pooled meta-analysis: the source studies use different tensor measures, spatial windows, regularization choices, and treatments of surface creep. A listed range is the range reported for that setting, not a common confidence interval, and the values should not be ranked directly as seismic hazard.

Table 2. Reported horizontal strain-rate values synthesized from the reviewed regional studies.

Region or structure	Reported value (nanostrain/yr)	Metric and spatial context	Interpretive qualification and source

Region or structure	Reported value (nanostrain/yr)	Metric and spatial context	Interpretive qualification and source
Southwestern Aegean	<10	Low horizontal strain in comparatively rigid areas	Upper-bound statement; offshore geometry limits coverage [2]
North Anatolian Fault	>=150	Fault-parallel shear / horizontal strain along most of the NAF	High-resolution InSAR-GNSS result; not a uniform locking rate [8]
East Anatolian Fault	50-80	Shear belt in the GNSS synthesis	Common regional range; mechanism may include transients [2]
EAF at Karliova	>100	Localized strain near the triple junction	Local value rather than a fault-wide range [2]
Ismetpasa segment (NAF)	>300	Apparent strain when surface creep is not represented as a discontinuity	Diagnostic model artefact; not stored elastic strain [2]
Greater Caucasus	>60	N-S to NNE-SSW shortening, increasing eastward	Sparse coverage limits fault-scale interpretation [2]
Pamir thrust system	-60 to -100	Dilatation; negative values denote shortening	Figure 2 plots the absolute magnitude (60-100) [2]
Pamir refined field	100-150	Strain norm in a refined inversion	Scale- and station-density-dependent [2]
Vakhsh Fault	130-170	Localized strain in the Pamir margin	Peak range in the refined field [2]
Central Tian Shan	50-60; local ~100	Regional strain with a localized peak	Typical and local values should be kept separate [2]
Haiyuan Fault (GNSS)	~60; local ~80	GNSS-derived fault-related strain	Broader effective resolution than the InSAR result [2]
Haiyuan Fault (InSAR)	>100; creep >400	Approximately 1 km strain field; very high value on a creeping reach	Strongly dependent on resolution and creep treatment [9]
Southern Tibetan rifts	>50	Local dilatation along seven N-S rifts	Separate from the summed extension of 18.4 +/- 1.7 mm/yr [12]
Himalayan arc	90-120	Arc-normal shortening above the MHT	Common belt-wide range; coupling varies along strike [2]
Eastern Himalayan syntaxis	~140; peaks ~170	Localized shortening / strain concentration	Local eastern increase, not an arc-wide value [2]

Sources: [2,8,9,12]. Values are reproduced as reported; metric type and scale qualifications are retained in the table.

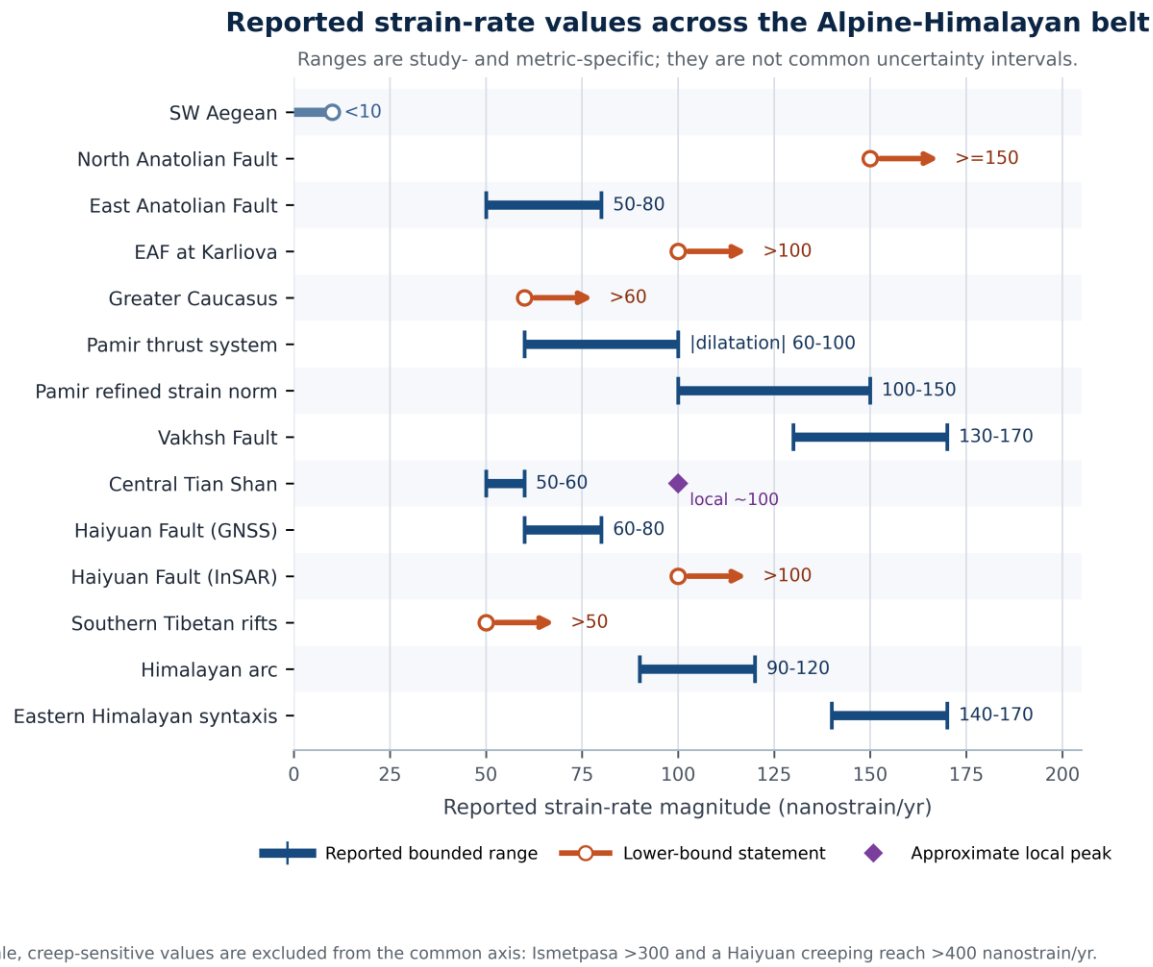

Figure 2. Comparison of reported strain-rate magnitudes. Solid intervals show bounded ranges; arrows denote lower-bound statements; the diamond marks a separate local peak. Metrics include shear, shortening, dilatation magnitude, and strain norm, so the figure supports comparison and retrieval rather than pooled ranking.

Source: compilation from Table 2 and [2,8,9,12].

5. What the new maps establish - and what they do not

5.1 A scale-dependent answer to block versus continuum deformation

At plate scale, velocities can often be described by rotating blocks and narrow boundaries. At tens of kilometers, the same blocks contain measurable strain; at kilometer scale, individual faults and creeping

Journal-status statement: It is not under-review at any journal. Subsequent versions may contain substantial revisions arising from community feedback / submission to journal(s). Co-author(s) may be included in future versions. Feedback is welcome & please feel free to contact the author for the same (via email only). PRE-PRINT VERSION (I): 31.08.2026

THIS MANUSCRIPT IS A NON-PEER-REVIEWED PREPRINT SUBMITTED TO EARTHARXIV.

reaches appear. The transcontinental field therefore does not select one universal rheological model. It shows where each approximation works. Rigid blocks remain useful for first-order kinematics, deformable blocks capture distributed interiors, and continuum models describe broad gradients without requiring every active structure to be known [1,2,11,13,37].

This scale dependence matters when comparing studies. A 100 km GNSS mesh and a 1 km InSAR-derived grid should not be ranked by peak strain alone. The finer model will usually return a narrower and higher gradient, while the broad model estimates the integrated motion more stably. A useful comparison reports both the peak and the velocity difference integrated across a standard-width profile.

5.2 Velocity gradients are mechanistically ambiguous

The regional examples above show why a surface velocity gradient is mechanistically ambiguous. At a strike-slip fault it may combine elastic loading with shallow creep, afterslip, or viscoelastic relaxation; across a collision front it may combine megathrust slip deficit with distributed deformation of the overriding plate. Hydrologic loading and processing ramps can generate similar gradients away from faults. Section 4.2 quantifies the creep-sensitive Ismetpasa case, and Section 4.5 describes the Himalayan coupling bias. Taken together, these examples establish the interpretive rule: strain rate is an observation-constrained descriptor, not a direct map of seismic potential.

5.3 Horizontal and vertical fields have different process mixtures

The strongest belt-wide horizontal patterns follow tectonic boundaries and distributed collision. The short-wave vertical field is different. Groundwater extraction dominates parts of Turkiye, Iran, and the North China Plain; compaction affects the Po Basin; permafrost and hydrology affect Tibet; and local landslides and mining occur throughout the belt [1,8-11,33,34]. Treating vertical velocity as the third tectonic component without process classification can corrupt both three-dimensional interpretation and horizontal strain through LOS decomposition.

5.4 An average velocity is not a stationary rate

The 2016-2024 transcontinental average is a powerful common baseline, but it spans multiple earthquakes, changes in satellite sampling, droughts, groundwater cycles, and cryosphere trends. A linear fit compresses these histories into one number. Where the underlying time series is nonlinear, its velocity

Journal-status statement: It is not under-review at any journal. Subsequent versions may contain substantial revisions arising from community feedback / submission to journal(s). Co-author(s) may be included in future versions. Feedback is welcome & please feel free to contact the author for the same (via email only). PRE-PRINT VERSION (I): 31.08.2026

THIS MANUSCRIPT IS A NON-PEER-REVIEWED PREPRINT SUBMITTED TO EARTHARXIV.

depends on the selected start and end dates. This limitation is especially relevant near the NAF and EAF, the Kunlun and Wenchuan post seismic zones, and rapidly changing aquifers or permafrost.

6. Spatial and observational gaps

GNSS coverage remains the most visible geographic inequality. Europe, the Aegean, and much of Turkiye support high-resolution strain inversions and near-fault tests. Coverage is thinner across Libya, Syria, Iraq, the northern Arabian plate, the Caucasus north of the Caspian, eastern Iran, Afghanistan, the Pamir, and long Himalayan and Tibetan sectors [2]. Political boundaries, data-access restrictions, security, power supply, and high-altitude logistics are part of the measurement problem. In these regions, a continentally complete raster can conceal a three-dimensional solution that is strongly inherited from interpolation.

InSAR gaps follow a different geography. Water removes the offshore portions of the Hellenic, Cyprus, and Makran subduction systems. Dense vegetation and monsoon moisture reduce coherence in the eastern Himalaya and Indochina. Seasonal snow and glaciers interrupt networks in the high Pamir, Karakoram, and Himalaya. Layover and shadow remove steep valley walls, and C-band phase can be dominated by permafrost or slope motion on the Tibetan Plateau. The weak sensitivity of standard Sentinel-1 geometry to north-south motion is particularly awkward because India-Asia convergence and many thrust-normal profiles are close to that direction.

Temporal completeness also varies. The loss of Sentinel-1B reduced revisit frequency after 2021, while regional archives begin and end at different dates. A frame with more acquisitions is not necessarily better if it includes a major transient that is modelled as a linear rate. Public release of displacement time series, valid-pixel masks, and acquisition metadata is therefore as important as the final velocity mosaic.

7. Integration challenges that now control interpretation

7.1 Common frame, common epoch, and common conventions

Every input must be traceable to a reference frame, epoch, sign convention, and uncertainty definition. A field labelled 'Eurasia-fixed' may have been obtained through different Euler poles or tie stations. LOS products may use opposite signs, and vertical GNSS rates may retain frame artefacts not present in horizontal components. The transcontinental achievement is as much a harmonization problem as a radar-processing problem [1,2,17].

7.2 Error covariance and weighting

InSAR pixels are not independent. Atmospheric structure, orbit ramps, DEM residuals, and shared interferograms produce spatial and temporal covariance. Treating millions of pixels as independent observations would overwhelm the much smaller GNSS data set numerically without adding equivalent information. Down sampling, covariance-based weighting, and spatially balanced sampling are required [15,16]. The residual covariance should be reported because it sets the confidence of long-wavelength deformation.

7.3 Atmospheric, orbital, and topographic residuals

Stratified tropospheric delay is often the largest InSAR error in high relief. Weather-model corrections and elevation-phase regressions reduce it, but performance varies across climate zones and for turbulent wavelengths [28,29,31]. Orbit errors and imperfect frame ties create broad ramps [30]. In Tibet, these effects overlap the long-wavelength tectonic signal and can be comparable to a few millimeters per year. No single correction should be accepted without before-after statistics and independent GNSS tests.

7.4 Discontinuities, transients, and surface processes

A smooth velocity basis is convenient but physically incomplete where a fault creeps at the surface. Conversely, allowing arbitrary discontinuities can fit unwrapping errors or field seams. Fault-aware inversions need mapped geometry, priors broad enough to permit new behavior, and diagnostics showing whether residuals improve. Time dependence is the complementary problem: coseismic steps, after slip, seasonal hydrology, and permafrost require explicit temporal basis functions rather than a single linear rate.

7.5 Resolution and hazard translation

The displayed grid, inversion mesh, smoothing length, and independent resolution are four different quantities. Publishing only the first encourages over-interpretation. Hazard use also requires translation from surface strain to fault slip deficit, stressing rate, seismogenic thickness, and moment accumulation,

Journal-status statement: It is not under-review at any journal. Subsequent versions may contain substantial revisions arising from community feedback / submission to journal(s). Co-author(s) may be included in future versions. Feedback is welcome & please feel free to contact the author for the same (via email only). PRE-PRINT VERSION (I): 31.08.2026

THIS MANUSCRIPT IS A NON-PEER-REVIEWED PREPRINT SUBMITTED TO EARTHARXIV.

with uncertainty propagated through each step [25,32]. Agreement between geodetic strain orientation and earthquake or stress tensors is encouraging [2,35], but orientation agreement does not establish recurrence or the timing of rupture.

8. Research priorities

8.1 Replace one average map with a four-dimensional deformation model

The next transcontinental product should retain displacement time series and estimate piecewise-linear, seasonal, coseismic, and post seismic terms. The purpose is not to add temporal complexity everywhere. It is to prevent a linear average from silently absorbing a transient and to identify where the rate changes. Common change-point tests across InSAR and continuous GNSS would make the interseismic interval an estimated quantity rather than an assumption.

8.2 Use complementary radar wavelengths and viewing geometries

Sentinel-1C and Sentinel-1D are now operational as the continuing C-band constellation [39]. Their renewed sampling should improve temporal coherence and shorten the interval needed to estimate velocity. NISAR entered routine science operations in early January 2026 [40], and NASA began public release of provisional L-band science products on 20 July 2026 [41]. L-band observations should be tested systematically in the vegetated Himalaya, Indochina, and seasonally decorrelating terrain, while C- and L-band differences can help diagnose shallow scattering and unwrapping behavior. Additional azimuth-offset, multiple-aperture interferometry, or non-polar viewing constraints are needed where north-south motion dominates.

8.3 Densify GNSS strategically, not uniformly

The largest gain will come from stations placed where LOS geometry is weak, reference ramps are uncertain, or competing fault models predict different velocities. Priorities include the Pamir-Hindu Kush, Greater Caucasus, Makran coast, Iran-Afghanistan transition, Himalayan syntaxes, and poorly instrumented Himalayan segments. Near-fault arrays and corner reflectors should target the distinction between creep and locking, while long-lived stations in stable interiors should strengthen the reference frame.

Journal-status statement: It is not under-review at any journal. Subsequent versions may contain substantial revisions arising from community feedback / submission to journal(s). Co-author(s) may be included in future versions. Feedback is welcome & please feel free to contact the author for the same (via email only). PRE-PRINT VERSION (I): 31.08.2026

THIS MANUSCRIPT IS A NON-PEER-REVIEWED PREPRINT SUBMITTED TO EARTHARXIV.

8.4 Publish resolution and covariance as first-class data

Each velocity and strain product should include valid-observation density, component-wise uncertainty, covariance or an operational approximation, resolution kernels or point-spread measures, and ensembles spanning defensible smoothing choices. Users could then integrate deformation across a fault-normal swath without mistaking correlated pixels for independent measurements. Benchmark regions with dense GNSS should be withheld during inversion and used for blind validation.

8.5 Separate tectonic and non-tectonic vertical motion by process

A generic high-pass or wavelength filter cannot distinguish groundwater compaction from fault-related uplift in every basin. The vertical field should be classified jointly with groundwater levels, GRACE and hydrologic models, precipitation, temperature, land cover, permafrost state, landslide inventories, and levelling. The result should retain the non-tectonic signal as a product rather than discard it as noise; aquifer depletion and slope instability are hazards in their own right.

8.6 Make fault-aware inversion the default comparison

For major faults, at least three models should be compared: a smooth continuum, a model with mapped velocity discontinuities, and a deformable-block or distributed-strain model. Creep, afterslip, and viscoelastic relaxation should have distinct temporal and spatial signatures. Model selection should use withheld GNSS and independent tracks, not only the fit to the data used in inversion. This comparison would turn the current block-continuum debate into a test of where and at what wavelength each representation is warranted.

8.7 Build a reproducible path from strain to seismic hazard

A belt-wide strain map becomes a hazard constraint only after separating elastic loading from creep and transient motion, assigning deformation to faults or distributed volumes, and comparing geodetic moment accumulation with earthquake and geological release. Regional studies in Nepal and Anatolia provide starting points [2,25]. The next step is a common probabilistic framework that carries observational covariance, model choice, seismogenic thickness, and off-fault deformation into the moment budget.

Journal-status statement: It is not under-review at any journal. Subsequent versions may contain substantial revisions arising from community feedback / submission to journal(s). Co-author(s) may be included in future versions. Feedback is welcome & please feel free to contact the author for the same (via email only). PRE-PRINT VERSION (I): 31.08.2026

THIS MANUSCRIPT IS A NON-PEER-REVIEWED PREPRINT SUBMITTED TO EARTHARXIV.

9. Conclusion

The first transcontinental Sentinel-1-GNSS products change the scale at which the Alpine-Himalayan belt can be studied. Average three-dimensional velocity and horizontal strain are now available on a common grid from the Alps to eastern China. The resulting picture is consistent across methods: major faults localize part of the motion, while broad regions between them continue to deform. Anatolia, the Pamir, the Himalayan front, and Tibetan fault systems contain narrow high-strain belts; Iran and parts of Tibet show extensive distributed strain; southern Tibet extends within an active collision; and much of the short-wavelength vertical signal comes from groundwater, permafrost, sediment, or slope processes rather than tectonics alone [1,2].

The central limitation is no longer the absence of measurements. It is the risk of assigning a precise tectonic meaning to a model-dependent gradient. North-south sensitivity, GNSS density, reference frames, time-window mismatch, atmospheric covariance, unwrapping, smoothing, and fault creep determine what a strain anomaly represents. A 1 km map is a major observational advance, but it is not a 1 km catalogue of independent fault loading.

The productive next step is a four-dimensional, multi-wavelength, uncertainty-aware framework in which velocity, strain, creep, transients, and non-tectonic vertical motion remain separable. Such a framework would preserve the continental perspective while making regional hazard interpretation harder to overstate and easier to test.

Acknowledgments

The author acknowledges the European Space Agency and the Copernicus Programme for maintaining the Sentinel-1 mission, and the teams that produced the published InSAR and GNSS products synthesized in this review.

Declarations

Author contributions. Mohit Sheode: conceptualization; literature curation; analysis and interpretation; visualization; writing - original draft; writing - review and editing.

Journal-status statement: It is not under-review at any journal. Subsequent versions may contain substantial revisions arising from community feedback / submission to journal(s). Co-author(s) may be included in future versions. Feedback is welcome & please feel free to contact the author for the same (via email only). PRE-PRINT VERSION (I): 31.08.2026

Funding. This research received no specific grant from any funding agency in the public, commercial, or not-for-profit sectors.

Conflicts of interest. The author declares no competing interests.

Data availability. No new primary datasets were generated or analyzed for this narrative review. All numerical values compiled in Table 2 and Figures 1-2 are drawn from the cited publications; the plotting values and their qualifications are reproduced in Table 2.

References

[1] Elliott JR, Fang J, Lazecky M, Maghsoudi Y, Ou Q, Payne JA, et al. Deformation, strains and velocities for the Alpine Himalayan Belt from trans-continental Sentinel-1 InSAR & GNSS. Remote Sensing of Environment. 2026; 338:115320. doi: 10.1016/j.rse.2026.115320

[2] Castro-Perdomo N, Jonsson S, Klinger Y, Masson F, Becker TW, Johnson K. Strain rates along the Alpine-Himalayan belt from a comprehensive GNSS velocity field. Journal of Geophysical Research: Solid Earth. 2025;130: e2025JB031738. doi:10.1029/2025JB031738

[3] McClusky S, Balassanian S, Barka A, Demir C, Ergintav S, Georgiev I, et al. Global Positioning System constraints on plate kinematics and dynamics in the eastern Mediterranean and Caucasus. Journal of Geophysical Research: Solid Earth. 2000;105(B3):5695-5719. doi:10.1029/1999JB900351

[4] Reilinger R, McClusky S, Vernant P, Lawrence S, Ergintav S, Cakmak R, et al. GPS constraints on continental deformation in the Africa-Arabia-Eurasia continental collision zone and implications for the dynamics of plate interactions. Journal of Geophysical Research: Solid Earth. 2006;111: B05411. doi:10.1029/2005JB004051

[5] Hatzfeld D, Molnar P. Comparisons of the kinematics and deep structures of the Zagros and Himalaya and of the Iranian and Tibetan plateaus and geodynamic implications. Reviews of Geophysics. 2010;48: RG2005. doi:10.1029/2009RG000304

[6] Lazecky M, Spaans K, Gonzalez PJ, Maghsoudi Y, Morishita Y, Albino F, et al. LiCSAR: An automatic InSAR tool for measuring and monitoring tectonic and volcanic activity. Remote Sensing. 2020;12(15):2430. doi:10.3390/rs12152430

[7] Morishita Y, Lazecky M, Wright TJ, Weiss JR, Elliott JR, Hooper A. LiCSBAS: An open-source InSAR time series analysis package integrated with the LiCSAR automated Sentinel-1 InSAR processor. Remote Sensing. 2020;12(3):424. doi:10.3390/rs12030424

[8] Weiss JR, Walters RJ, Morishita Y, Wright TJ, Lazecky M, Wang H, et al. High-resolution surface velocities and strain for Anatolia from Sentinel-1 InSAR and GNSS data. Geophysical Research Letters. 2020;47: e2020GL087376. doi:10.1029/2020GL087376

[9] Ou Q, Daout S, Weiss JR, Shen L, Lazecky M, Wright TJ, et al. Large-scale interseismic strain mapping of the NE Tibetan Plateau from Sentinel-1 interferometry. Journal of Geophysical Research: Solid Earth. 2022;127(6): e2022JB024176. doi:10.1029/2022JB024176

[10] Watson AR, Elliott JR, Lazecky M, Maghsoudi Y, McGrath JD, Walters RJ. An InSAR-GNSS velocity field for Iran. Geophysical Research Letters. 2024;51(10):e2024GL108440. doi:10.1029/2024GL108440

[11] Liu C, Ji L, Zhu L, et al. Kilometer-resolution three-dimensional crustal deformation of Tibetan Plateau from InSAR and GNSS. Science China Earth Sciences. 2024; 67:1818-1835. doi:10.1007/s11430-023-1289-4

[12] Chen H, Qu C, Zhao D, Shan X, Li C, Dal Zilio L. Large-scale extensional strain in Southern Tibet from Sentinel-1 InSAR and GNSS data. Geophysical Research Letters. 2024;51(19): e2024GL110512. doi:10.1029/2024GL110512

[13] Fang J, Wright TJ, Johnson KM, Ou Q, Styron R, Craig TJ, et al. Strain partitioning in the Southeastern Tibetan Plateau from kinematic modeling of high-resolution Sentinel-1 InSAR and GNSS. Geophysical Research Letters. 2024;51: e2024GL111199. doi:10.1029/2024GL111199

[14] Shen ZK, Liu Z. Integration of GPS and InSAR data for resolving three-dimensional crustal deformation. Earth and Space Science. 2020;7: e2019EA001036. doi:10.1029/2019EA001036

[15] Wei M, Sandwell D, Smith-Konter B. Optimal combination of InSAR and GPS for measuring interseismic crustal deformation. Advances in Space Research. 2010;46(2):236-249. doi: 10.1016/j.asr.2010.03.013

[16] Parizzi A, Gonzalez FR, Brcic R. A covariance-based approach to merging InSAR and GNSS displacement rate measurements. Remote Sensing. 2020;12(2):300. doi:10.3390/rs12020300
[17] Lemrabet L, Doin MP, Lasserre C, Durand P. Referencing of continental-scale InSAR-derived velocity fields: Case study of the eastern Tibetan Plateau. Journal of Geophysical Research: Solid Earth. 2023;128: e2022JB026251. doi:10.1029/2022JB026251
[18] Wang H, Wright TJ, Liu-Zeng J, Peng L. Strain rate distribution in south-central Tibet from two decades of InSAR and GPS. Geophysical Research Letters. 2019;46: e2019GL081916. doi:10.1029/2019GL081916
[19] Zhao D, Qu C, Burgmann R, Gong W, Shan X, Qiao X, et al. Large-scale crustal deformation, slip-rate variation, and strain distribution along the Kunlun Fault (Tibet) from Sentinel-1 InSAR observations (2015-2020). Journal of Geophysical Research: Solid Earth. 2022;127(1):e2021JB022892. doi:10.1029/2021JB022892
[20] Nocquet JM, Sue C, Walpersdorf A, Tran T, Lenotre N, Vernant P, et al. present-day uplift of the western Alps. Scientific Reports. 2016; 6:28404. doi:10.1038/srep28404
[21] Nocquet JM. Present-day kinematics of the Mediterranean: A comprehensive overview of GPS results. Tectonophysics. 2012; 579:220-242. doi: 10.1016/j.tecto.2012.03.037
[22] Jade S, Mukul M, Gaur VK, Kumar K, Shrungeshwara TS, Satyal GS, et al. Contemporary deformation in the Kashmir-Himachal, Garhwal and Kumaon Himalaya: Significant insights from 1995-2008 GPS time series. Journal of Geodesy. 2014;88(6):539-557. doi:10.1007/s00190-014-0702-3
[23] Kundu B, Yadav RK, Bali BS, Chowdhury S, Gahalaut VK. Oblique convergence and slip partitioning in the NW Himalaya: Implications from GPS measurements. Tectonics. 2014;33(10):2013-2024. doi:10.1002/2014TC003633
[24] Panda D, Lindsey EO. Overriding plate deformation controls inferences of interseismic coupling along the Himalayan megathrust. Journal of Geophysical Research: Solid Earth. 2024;129: e2024JB029819. doi:10.1029/2024JB029819
[25] Verma H, Sharma Y, Ching KE, Pasari S. Contemporary seismic moment budget along the Nepal Himalaya derived from high-resolution InSAR and GPS velocity field. Acta Geophysica. 2025;73(1):171-186. doi:10.1007/s11600-024-01411-6
[26] Mohanty A, Gahalaut VK, Chowdhury S, et al. Geodetic constraints on slip rate on the Karakoram Fault and its role in Himalayan arc deformation. Earth and Planetary Science Letters. 2024; 623:118512. doi: 10.1016/j.epsl.2023.118512
[27] Yadav RK, Gahalaut VK, Bansal AK. Tectonic and non-tectonic crustal deformation in Kumaun Garhwal Himalaya. Quaternary International. 2021; 585:171-182. doi: 10.1016/j.quaint.2020.10.011
[28] Doin MP, Lasserre C, Peltzer G, Cavalie O, Doubre C. Corrections of stratified tropospheric delays in SAR interferometry: Validation with global atmospheric models. Journal of Applied Geophysics. 2009; 69:35-50. doi: 10.1016/j.jappgeo.2009.03.010
[29] Jolivet R, Grandin R, Lasserre C, Doin MP, Peltzer G. Systematic InSAR tropospheric phase delay corrections from global meteorological reanalysis data. Geophysical Research Letters. 2011;38: L17311. doi:10.1029/2011GL048757
[30] Fattahi H, Amelung F. InSAR uncertainty due to orbital errors. Geophysical Journal International. 2014; 198:549-568. doi:10.1093/gji/ggu276
[31] Kinoshita Y. Development of an InSAR neutral atmospheric delay correction model using GNSS zenith total delay and its horizontal gradient. IEEE Transactions on Geoscience and Remote Sensing. 2022; 60:5231414. doi:10.1109/TGRS.2022.3188988
[32] Maurer J, Materna K. Quantification of geodetic strain rate uncertainties and implications for seismic hazard estimates. Geophysical Journal International. 2023;234(3):2128-2142. doi:10.1093/gji/ggad191
[33] Fan C, Liu L, Zhao Z, Mu C. Pronounced underestimation of surface deformation due to unwrapping errors over Tibetan Plateau permafrost by Sentinel-1 InSAR: Identification and correction. Journal of Geophysical Research: Earth Surface. 2025;130: e2024JF007854. doi:10.1029/2024JF007854
[34] Daout S, Dini B, Haeberli W, Doin MP, Parsons B. Ice loss in the northeastern Tibetan Plateau permafrost as seen by 16 years of ESA SAR missions. Earth and Planetary Science Letters. 2020; 545:116404. doi: 10.1016/j.epsl.2020.116404
[35] Pietrolungo F, Lavecchia G, Madarieta-Txurruka A, et al. Comparison of crustal stress and strain fields in the Himalaya-Tibet region: Geodynamic implications. Remote Sensing. 2024;16(24):4765. doi:10.3390/rs16244765
[36] Su X, Bao Q, Gao Z, Huang J. Three-dimensional interseismic crustal deformation in the northeastern margin of the Tibetan Plateau using GNSS and InSAR. Journal of Asian Earth Sciences. 2024; 276:106328. doi: 10.1016/j.jseaes.2024.106328
[37] England P, Molnar P. Late Quaternary to decadal velocity fields in Asia. Journal of Geophysical Research: Solid Earth. 2005;110: B12401. doi:10.1029/2004JB003541
[38] Wang H, Wright TJ. Satellite geodetic imaging reveals internal deformation of western Tibet. Geophysical Research Letters. 2012;39: L07303. doi:10.1029/2012GL051222
[39] European Space Agency. Sentinel-1D goes live: a milestone for Europe's radar mission. 1 May 2026. Available online (accessed 31 August 2026).
[40] NASA. NISAR mission overview - quick facts. Updated 2026. Available online (accessed 31 August 2026).

Journal-status statement: It is not under-review at any journal. Subsequent versions may contain substantial revisions arising from community feedback / submission to journal(s). Co-author(s) may be included in future versions. Feedback is welcome & please feel free to contact the author for the same (via email only). PRE-PRINT VERSION (I): 31.08.2026

THIS MANUSCRIPT IS A NON-PEER-REVIEWED PREPRINT SUBMITTED TO EARTHARXIV.

[41] NASA Earthdata. NISAR L-Band Data Now Publicly Available. 21 July 2026. Available online (accessed 31 August 2026).